Available online at www.sciencedirect.com
ScienceDirect
Magnetic Resonance Imaging 25 (2007) 1155–1161
MAGNETIC RESONANCE IMAGING

Fast multivoxel two-dimensional spectroscopic imaging at 3 T☆

Dong-Hyun Kim[a,b,*], Roland Henry[a], Daniel M. Spielman[c]

[a]Department of Radiology, University of California–San Francisco, San Francisco, CA, USA
[b]School of Electrical and Electronic Engineering, Yonsei University, Seoul 120-749, South Korea
[c]Department of Radiology, Stanford University, Stanford, CA, USA

Received 26 September 2006; revised 24 January 2007; accepted 28 January 2007

Abstract

The utility of multivoxel two-dimensional chemical shift imaging in the clinical environment will ultimately be determined by the imaging time and the metabolite peaks that can be detected. Different k-space sampling schemes can be characterized by their minimum required imaging time. The use of spiral-based readout gradients effectively reduces the minimum scan time required due to simultaneous data acquisition in three k-space dimensions (k_x, k_y and k_{f_2}). A 3-T spiral-based multivoxel two-dimensional spectroscopic imaging sequence using the PRESS excitation scheme was implemented. Good performance was demonstrated by acquiring preliminary in vivo data for applications, including brain glutamate imaging, metabolite T_2 quantification and high-spatial-resolution prostate spectroscopic imaging. All protocols were designed to acquire data within a 17-min scan time at a field strength of 3 T.

Keywords: Magnetic resonance spectroscopic imaging; Spiral readout gradients; 2D J-resolved spectroscopy

1. Introduction

In vivo proton magnetic resonance spectroscopy provides valuable information regarding biochemical processes. The spectroscopic information content can be enriched in several different ways. Short echo time (TE) spectroscopy (TE ≤35 ms) has been extensively used to enable the robust quantification of metabolites with both long and short T_2 relaxation times. Magnetic resonance spectroscopic imaging (MRSI) can provide additional topological knowledge. In addition, two-dimensional (2D) spectroscopy can be used to better detect J-coupled metabolites [1–3]. While short echo magnetic resonance spectroscopy can be implemented without sacrificing scan times, multidimensional techniques typically require longer scan times to gather the desired information. This additional data acquisition can be formulated as extended k-space coverage. In the case of MRSI, the coverage is represented as k_x, k_y and k_z, while 2D spectroscopy requires sampling in both the k_{f_1} (=t_1: indirect evolution time, Fourier domain of f_1) and k_{f_2} (=t_2: direct detection time, Fourier domain of f_2) dimensions.

Approaches that combine MRSI with 2D spectroscopy have recently been introduced [4–8]. These multivoxel 2D spectroscopic imaging techniques can gather spatial distributions of metabolites with complex coupled spectra. Despite the prospect of many new applications, the necessary overwhelming increase in scan time hampers the clinical use of these techniques. The requirements to acquire data in three-dimensional (3D) spatial coverage and 2D spectral coverage can be expressed in five k-space axes, namely, k_{f_1}, k_{f_2}, k_x, k_y and k_z. Conventional phase-encoded MRSI methods are too inefficient for most applications, although longer scan times are inevitable due to the signal-to-noise ratio (SNR) requirements in some cases [7]. An alternative method incorporates fast imaging features, thereby reducing the overall minimum scan time [9–13].

We investigated fast imaging techniques combined with 2D spectroscopic imaging. Using a k-space sampling efficiency criterion, we found that oscillating readout gradients, especially those generating a spiral k-space trajectory, had relatively short minimum scan time requirements. This feature makes it possible to perform clinical in vivo multivoxel 2D spectroscopic imaging within acceptable scan times. Expanding on our previous results [9,11],

☆ This study was supported by the National Institutes of Health through Grant Nos. CA48269 and RR09784.

* Corresponding author. School of Electrical and Electronic Engineering, Yonsei University, Seoul 120-749, South Korea. Tel.: +82 2 2123 5874.
E-mail address: donghyunkim@yonsei.ac.kr (D.-H. Kim).

0730-725X/$ – see front matter © 2007 Elsevier Inc. All rights reserved.
doi:10.1016/j.mri.2007.01.118

we applied the technique to various new applications, including volumetric TE-averaged MRSI of brain glutamate (Glu) levels, volumetric multi-TE MRSI for T_2 quantification and high-spatial-resolution multivoxel 2D *J*-resolved MRSI to detect citrate and polyamines in the prostate at 3 T.

2. Methods

2.1. k-space sampling efficiency

The *k*-space sampling efficiency is determined by the minimum number of repetition time (TR) steps required for a scan protocol. Given an imaging matrix size of $N \times N$, the minimum number of TR steps for conventional phase-encoded MRSI and that for echoplanar (EP) MRSI will be N^2 and N, respectively. For 2D spectroscopy requiring multiple TE acquisitions, the total scan time is linearly proportional to the number of TE steps. Spectroscopic U-FLARE approaches have a total scan time that is largely independent of the matrix size N but dependent on the spectral bandwidth and resolution in f_2 [14].

To evaluate the minimum number of TR steps for the spiral protocol, we used the trajectory design method presented by Glover [15] and simulated the required length of the spirals for various values of N. Simulations were performed assuming a spectral bandwidth of 1000 Hz in f_2. For spirals, the number of TR steps is governed by the number of spatial interleaving steps required. Spatial interleaving is needed in reducing the length of each spiral to fulfill the spectral bandwidth requirements. Each spiral during a single readout (TR period) is connected via rewinder gradients that are designed to relocate the *k*-space trajectory back to its origin (i.e., $k_{xy}=0$). These additional rewinder gradients also cause a reduction in the spectral bandwidth. To reduce the length of these rewinders as much as possible, we used a gradient design algorithm that operates at the gradient amplifier slew-rate limit. A second-order polynomial fit of the minimum number of TR steps required was calculated for the given values of N.

2.2. In vivo studies

Spiral readout gradients with 2D spectroscopy features were added to a PRESS sequence as shown in Fig. 1. Three protocols were used to validate the sequence for specific applications. All scans were conducted on a 3-T EXCITE scanner (General Electric Healthcare Technologies, Milwaukee, WI, USA).

2.2.1. Experiment 1: Volumetric (3D) imaging of brain Glu, creatine, choline and N-acetylaspartate

The TE-averaging approach was used with nine TEs chosen to maximize Glu C_4 proton peak detection at 2.35 ppm [16,17]. Single-voxel spectroscopy was performed using a phantom containing Glu at various TEs with a high SNR to estimate the Glu C_4 amplitude. TEs in regions with relatively big Glu C_4 amplitudes were densely selected. As a result, the TE steps chosen had a sampling density that was proportional to the amplitude of the Glu C_4 proton peak. Specifically, the TEs chosen for this study were 40, 50, 65, 85, 110, 140, 170, 200 and 220 ms. The spectroscopic imaging parameters were as follows: 16×16×8 spatial coverage over a 16×16×12-cm field of view (FOV; nominal spatial resolution of 1.5 cc); 1.7-s TR; two signal averages; CHESS water suppression; approximately 1000-Hz spectral bandwidth in f_2 acquired with 512 points; and 16.5-min scan time using an eight-channel phased-array head receiver coil. Phase encoding in z was performed to obtain resolution in the through-plane direction. The spatial selection of the PRESS box was a rectangular region within the parenchyma of the brain typically of an approximate size of 12×12×8=1152 cc. Spatial saturation pulses were applied to eliminate lipid contamination and aliasing due to the relatively small FOV. An eddy current correction routine as outlined in Ref. [18] was used to reduce the effects of gradient imperfections for this particular spiral trajectory. For Experiments 2 and 3, no correction routine was used since the spiral trajectories did not cause detectable amounts of error. Raw data collected from the different TEs were first added to obtain TE-averaged raw data. The data were then reconstructed by applying gridding in k_x and k_y. Following gridding, a four-dimensional fast Fourier transform (FFT) was performed to convert data from the k_x, k_y, k_z and k_{f_2} ($=t_2$) domains to the spatial x,y,z and spectral f_2 domains, respectively. Apodization using a 4-Hz Lorentzian filter was applied prior to the FFT in the t_2 domain. A repeatability study was also performed on a volunteer to evaluate the technique's potential for use in clinical settings.

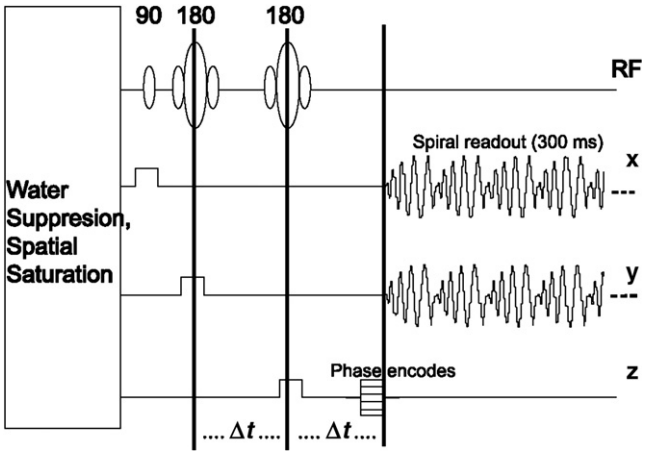

Fig. 1. Pulse sequence diagram. A conventional PRESS excitation sequence was used with spiral readout gradients to provide efficient *k*-space coverage. Resolution in the third spatial dimension (z) was obtained using phase-encoded gradients, which were usually played out simultaneously with crusher gradients (not shown in this diagram). The short minimum scan times allow for the acquisition of additional information by varying Δt, which encodes for TE-dependent modulations (*J*-coupling) and T_2.

2.2.2. Experiment 2: Simultaneous multivoxel metabolite T2 quantification

For this application, the imaging parameters were slightly modified from those given above: 8×8×8 spatial coverage over a 16×16×8-cm FOV (nominal spatial resolution of 4 cc); 2-s TR; one signal average; CHESS water suppression; approximately 1000-Hz spectral bandwidth in f_2 acquired with 512 points; TE from 40 to 190 ms with 10-ms intervals for 16 TE step acquisitions; and 17-min scan time. A spiral out–in trajectory was used for the readout in this case, which reduces phase errors due to gradient moment buildup during the readout [19]. Phase encoding in z was used for through-plane coverage. The spatial selection of the PRESS box was normally chosen to be approximately 12×12×6=864 cc, and the positioning of the spatial saturation pulses was similar to that in Experiment 1. This study was also performed using an eight-channel phased-array coil. For the studies using multichannel receivers, data were processed for individual coils separately and then in combination. Prior to combination, each voxel from each coil was multiplied by a weighting factor proportional to the amplitude of the phased water spectra. For Experiments 1 and 2, higher-order shimming over the selected region was performed to improve field homogeneity [20]. For this experiment, data were reconstructed separately for each TE acquisition, much like the procedure outlined for Experiment 1. From each reconstructed TE data, the areas of N-acetylaspartate (NAA), creatine (Cr) and choline (Cho) were calculated and curve fitting of the area values was performed using a single exponential decay model to estimate the T_2 values for every voxel.

2.2.3. Experiment 3: High-spatial-resolution multivoxel 2D J-resolved MRSI for prostate imaging

Spiral trajectories are characterized as having a scan time that is largely independent of the imaging matrix and FOV. The protocol was modified for obtaining fine spatial resolution without an increase in the minimum scan time or a decrease in FOV [11]. The modified imaging parameters for single-slice high-spatial-resolution 2D J-resolved MRSI were as follows: 32×32 in-plane matrix size over a 16-cm FOV with 1-cm slice thickness (nominal spatial resolution of 0.25 cc); 16 TE steps starting from 35 to 285 ms with 15.6-ms intervals (64-Hz bandwidth and 4-Hz resolution in f_1); approximately 1000-Hz spectral bandwidth in f_2 acquired with 256 points; two signal averages; 2-s TR; and 17-min scan time. An endorectal coil was used for signal reception. Following gridding in k_x and k_y, a five-dimensional FFT was performed to convert data from the k_x, k_y, k_z, k_{f_1} (=t_1) and k_{f_2} (=t_2) domains to the spatial x,y,z and spectral f_1 and f_2 domains, respectively. Data from the five-dimensional reconstructed data sets were visualized for particular f_1 values. In particular, spectra corresponding to the f_1=0 and −8 Hz lines [J(0) Hz and J(−8) Hz lines] were extracted and phased manually to investigate the presence of the metabolites of interest.

3. Results

Fig. 2 shows the minimum required TR steps for different MRSI sequence protocols assuming a single TE acquisition. Note that further reductions of this value could be achieved by using other approaches such as parallel imaging schemes and reduced k-space sampling trajectories [21–23]. The resulting polynomial fit indicated that the number of TR steps required for a given imaging matrix size of $N\times N$ for spiral acquisitions was $0.012\times N^2+1$. Compared with EP spectroscopic imaging (EPSI) acquisitions, spirals require approximately half the scan time for the given matrix sizes.

An example of volumetric TE-averaged MRSI from a patient suspected of having amyotrophic lateral sclerosis is shown in Fig. 3. Representative spectra from the 16×16×8 TE-averaged data set are shown covering the corticospinal tract. The largest Glu concentrations were observed in the gray matter regions (indicated by a V sign). A repeatability study performed on a healthy volunteer resulted in the following coefficients of variation (CV): NAA≈7%; Cr≈10.8%; and Cho≈10.6%. For Glu, the CV was approximately 17% in regions where Glu values were clearly visible, such as those shown in the left column of Fig. 3. These regions were mostly located in the gray matter region as indicated in Fig. 3. Note that reduced B_0 homogeneity resulted in broadened line widths in the inferior and anterior voxels.

Fig. 4 shows an example of metabolite T_2 quantification via spiral 2D MRSI from a healthy volunteer. From the

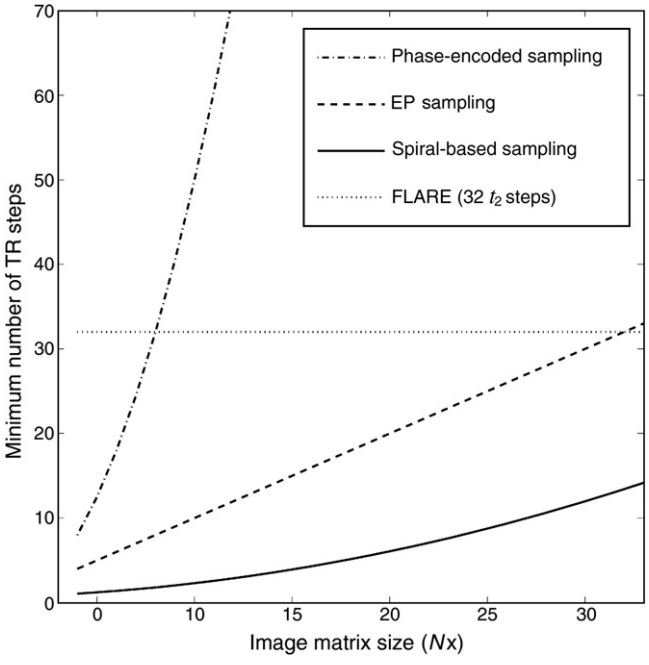

Fig. 2. The minimum number of TR steps required given an imaging matrix size of $N\times N$. The EP and spiral sampling acquisitions were simulated assuming a spectral bandwidth of 1000 Hz. For the spectroscopic FLARE acquisition, 32 steps in the t_2 direction were assumed, governing the minimum scan time.

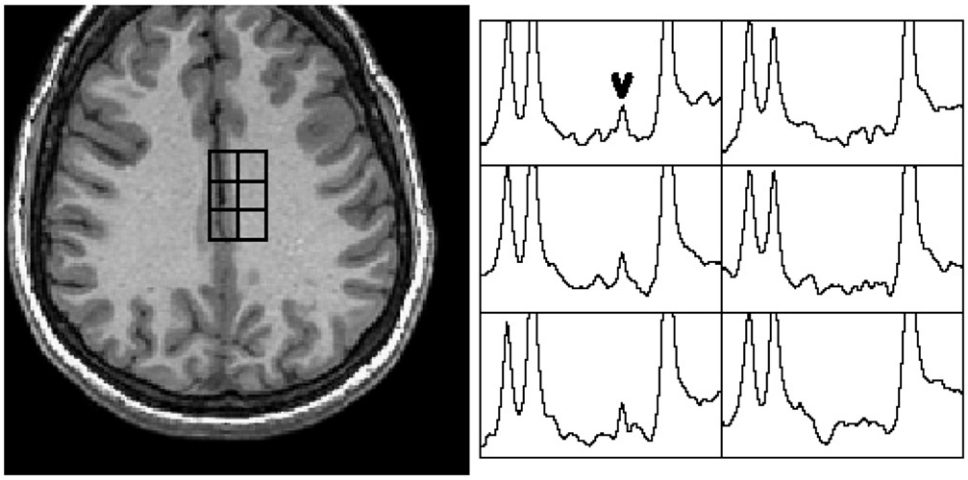

Fig. 3. Volumetrically resolved TE-averaged spectra. TE averaging was performed over a 3D spatial coverage using spiral readout gradients. Metabolite spectra from the 1.5- to 3.7-ppm region of the TE-averaged acquisition are shown. Glu, mostly seen from the gray matter, is indicated with a *V* sign. Note that the actual spatial dimension resolved was 16×16×8. Only a small portion of the spectra covering the corticospinal tract is displayed.

processed data sets, the voxels containing most gray and white matter areas were selected and are shown with (a) corresponding TE spectra, (b) summed (TE averaged) spectra and (c) T_2 fitting example. The T_2 estimates in the gray and white matter regions were 199 and 278 ms for NAA, 144 and 140 ms for Cr and 299 and 397 ms for Cho [16].

Finally, Fig. 5 displays an example of high-resolution 2D *J*-resolved prostate MRSI from a subject suspected of

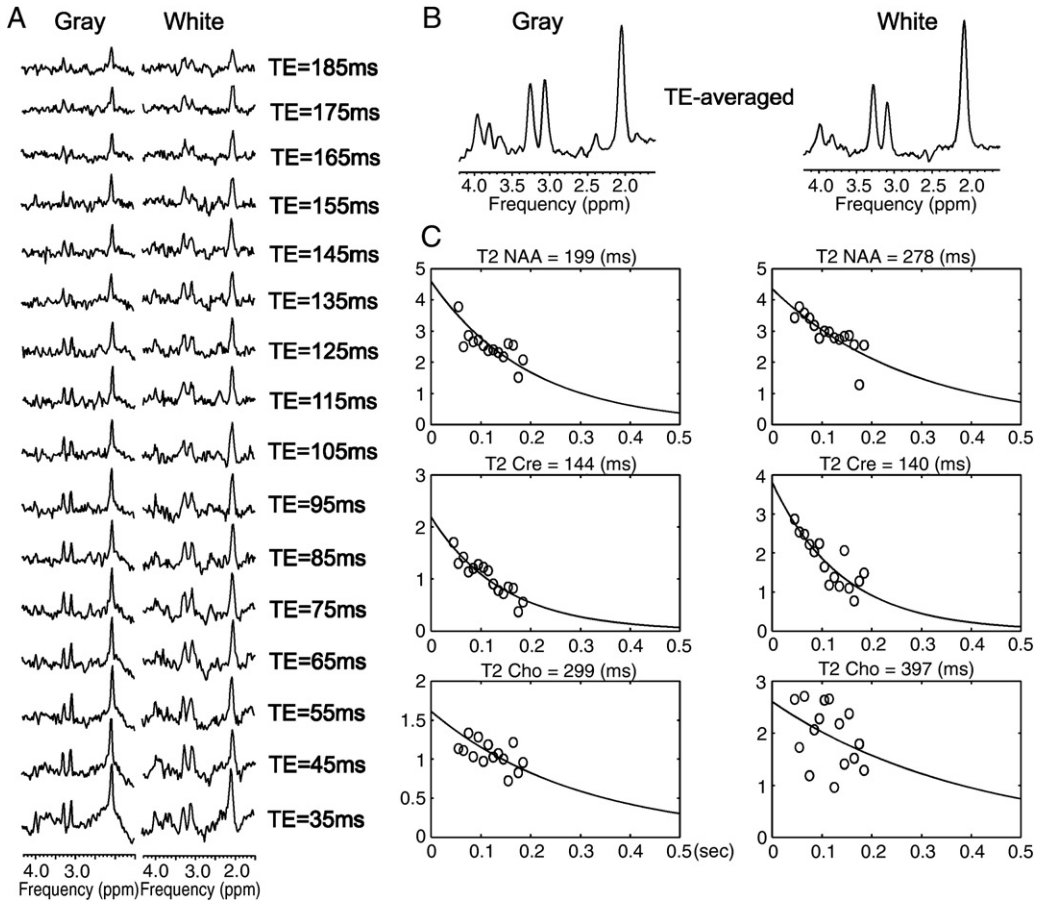

Fig. 4. Singlet metabolite T_2 values. Two voxels from mostly gray and white matter regions were chosen for this example. The T_2 value was within 10% of previously published values for normal gray and white matter regions. Although only two voxels were selected for T_2 calculations in this case, the ability to acquire volumetric data and simultaneously measure T_2 for each voxel can provide significantly important biochemical information about metabolite characteristics. (A) Individual spectra at corresponding TE values, (B) TE-averaged spectra, and (C) T_2 quantification.

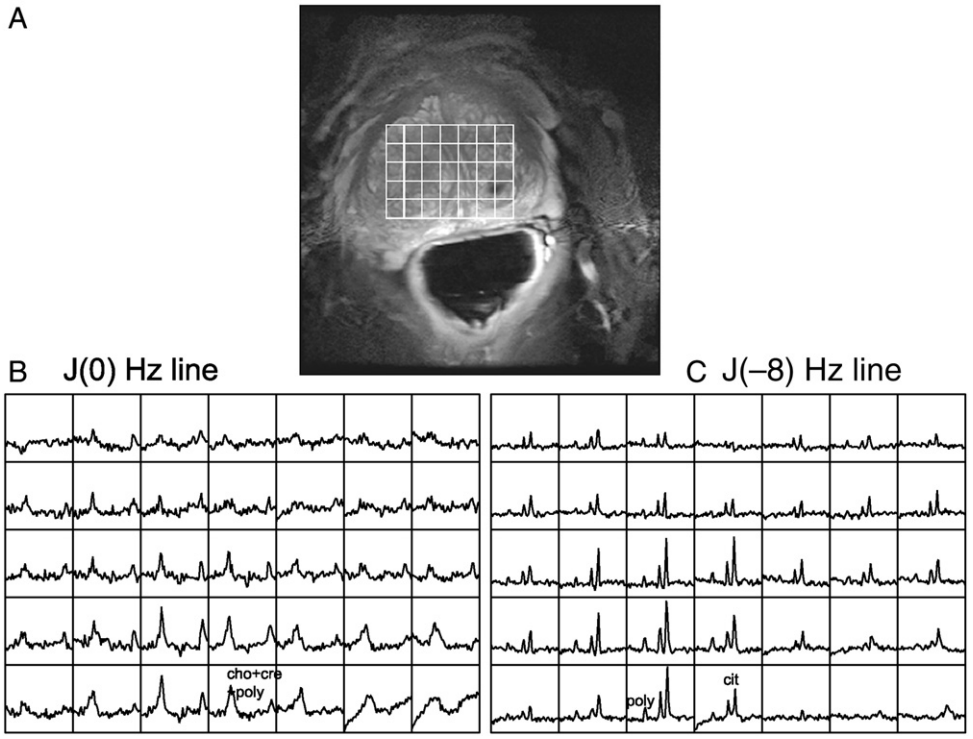

Fig. 5. (A) Single-slice *J*-resolved MRSI of the prostate at a high spatial resolution (0.25 cc). Whereas citrate resonance was hardly detectable while polyamines overlapped with Cho and Cr in the *J*(0) Hz line spectra (B), the use of *J*-resolved spectroscopy led to the detection of polyamine and citrate in the *J*(−8) Hz line spectra (C). All spectra shown are in the absorption mode following manual phasing.

having prostate cancer. It has previously been shown that the addition of a *J*-resolved dimension allows for observation of the *J*-modulation of citrate and the resolution of polyamines from overlapping Cho and Cr signals [24]. These *J*-modulated signals can be clearly seen in this example from the *J*(−8) Hz line spectra, which show the polyamine and doublet citrate metabolite. In addition, the spatial distribution of these signal components is well resolved at a high spatial resolution of 0.25 cc. It is worth noting that applying the same imaging parameters would have necessitated scan times of 1092 and 34 min for conventional phase-encoded MRSI and EP MRSI, respectively.

4. Discussion

We implemented and demonstrated 3-T multivoxel 2D MRSI sequences using spiral readout gradients for several applications. The application of spiral *k*-space trajectories, which use two simultaneously oscillating readout gradients, reduced the minimum number of TR steps needed as compared with other acquisition methods. This method can be effectively added to 2D spectroscopic acquisitions while maintaining high spectral quality and reasonable scan times. Our methods were all devised to be executed within a reasonable scan time of approximately 17 min with a TR value of 1.7 or 2 s. Given this protocol (matrix size $N=16$), the imaging times required for conventional phase-encoded MRSI and EPSI would be ×64 and ×4, respectively, of the imaging time for spiral MRSI, as shown in Fig. 2. Previous studies on 2D MRSI using spiral readouts were limited in spatial coverage or spatial resolution [9,11]. We have extended these studies by gathering volumetric 3D data or high-spatial-resolution single-slice data sets. Imaging on a 3-T scanner using multiple receiver coils facilitated the utility of this technique by providing an improved SNR.

The ability to simultaneously perform 2D spectroscopy and spectroscopic imaging within a reasonable scan time has great potential for clinical applications. For TE-averaged volumetric MRSI, we demonstrated the measurement of the spatial distribution of brain Glu. In this implementation, we have used a variable density filter function approach in which the TE steps were optimized for Glu C_4 detection. Different filter functions could also be used to enhance the detection of other metabolites, such as GABA and myo-inositol [25]. Although the CVs of NAA, Cr and Cho were within reasonable values, the CV for Glu was relatively high owing to the low SNR achieved for this metabolite, which is dominated by the voxel size prescribed. Another reason for the high CV of Glu is the low spatial resolution of the multivoxel acquisition, which leads to ringing effects. The remaining lipids after imperfect suppression became a large source of contamination due to ringing. Lipids themselves are coupled resonances leading to a strong TE dependence that can overwhelm Glu

behavior. Improved lipid suppression pulses need to be developed for volumetric coverage applications.

The ability to quantify metabolite T_2 from various regions of the brain simultaneously in a single scan can reduce systematic problems in multiple studies while greatly increasing the scan's efficiency. Volumetrically resolved T_2 quantification can be very useful in providing not only new information regarding local magnetic environments but also improved absolute metabolite quantification. While most quantification approaches rely on reported T_1 and T_2 values, applications such as pediatrics, in which dramatic changes in the parenchymal environment occur during the early stages of life, could incur substantial errors when using assumed and fixed relaxation values [26]. The capability to measure T_2 spatial variations directly will certainly help in the quantification process. It is worth noting that T_2 information can be obtained automatically in both TE-averaged spectroscopy and *J*-resolved 2D spectroscopy since raw data are stored separately for each TE acquisition.

One limitation of our procedure for multivoxel T_2 measurements, as illustrated in the example shown in Fig. 4, is the relatively big voxel size, which leads to inaccurate quantification due to signal contamination from adjacent voxels. Although we selected the voxels with the purest gray and white matter components, contributions from outside the target voxels are unavoidable. Another difficulty is the long process time needed to calculate the area of each metabolite and to estimate the T_2 values for every voxel, thereby limiting the number of case studies. At the time of this study, we did not have an automated procedure for this routine. We are currently incorporating a multivoxel multiecho LC-Model fitting routine [27] to automate the whole reconstruction and fitting procedure. In this example, the scatter of the Cho peak should be noted. Although we are not sure of the source of this scatter, a potential explanation is that the peak at 3.2 ppm reflects the contribution of a multitude of metabolites, including myo-inositol and taurine, in addition to Cho [28]. The amount of scatter would then be dependent on the selected TEs due to the strong coupling effects of both myo-inositol and taurine.

The utility of multivoxel 2D MRSI is not limited to the functions presented here. Indeed, given the flexible scan time management of the spirals, other applications are also possible. In the examples presented, we have generally used a small number of TE steps ($\leq$16), which undersamples the f_1 spectra and results in a small spectral bandwidth. Other researchers have shown that oversampled *J*-resolved acquisitions can be very useful for reducing side lobes arising from unsuppressed water or lipid resonances [29,30]. Our approach could be extended to perform oversampling of the f_1 domain. In this case, however, decreased spatial resolution may be unavoidable to reduce the overall scan time to within clinically acceptable limits.

In practice, several major obstacles can arise during the actual implementation of multivoxel 2D MRSI. High gradient performance is particularly important. The use of oscillating gradients in EPSI or spiral-based MRSI can be demanding on the gradient coils. For Experiment 1, we used an eddy current correction routine in addition to the pre-emphasis routine provided by the scanner itself to further mitigate these effects. For the other experiments, our eddy current correction routine did not help, as explained in Ref. 18. The collection of multi-TE data directly impacts the amount of acquired data with typical raw data file sizes often exceeding 1 GB, which can be demanding on the scanner acquisition and reconstruction hardware. In fact, this was the reason why we could not gather additional TE data for Experiment 1, for which we opted to use two signal averages instead due to the raw data size limit.

Finally, there are general differences in the performance of spiral-based MRSI, EP MRSI and conventional phase-encoded MRSI. As mentioned, EPSI and spiral trajectories demand high performance gradients. Depending on gradient fidelity and specific spiral trajectories, we have seen spectral differences of up to approximately 10% in previous studies [18]. For EPSI, gradient coil dependence can be somewhat alleviated by using flyback EP trajectories [31]. The relative sensitivity to lipids or inhomogeneity is governed by the impulse response of these trajectories. While MRSI itself will resolve for any inhomogeneity, the resulting end image will be different for these trajectories, which depend on the spatial point spread function [32]. In relation to motion sensitivity, spirals are considered advantageous due to their sampling pattern, which starts at the *k*-space origin. More comprehensive studies comparing these schemes have been published and showed small SNR differences between EPSI and phase-encoded methods [33]. We have recently added the spiral trajectory to the aforementioned study [33], and the results indicated that the performance of spiral trajectories is similar to that of EPSI trajectories (data not shown).

5. Conclusions

We investigated the utility of a variety of multivoxel 2D MRSI sequences. The use of spiral readout gradients leads to a small number of TR steps, enabling clinically feasible scan times. Applications of this technique include brain Glu mapping, metabolite T_2 mapping and improved prostate MRSI.

References

[1] Ryner LN, Sorenson JA, Thomas MA. Localized 2D *J*-resolved 1H MR spectroscopy: strong coupling effects in vitro and in vivo. Magn Reson Imaging 1995;13(6):853–69.

[2] Aue WP, Karhan J, Ernst RR. Homonuclear broadband decoupling and two-dimensional *J*-resolved NMR spectroscopy. J Chem Phys 1976;64:4226.

[3] Dreher W, Leibfritz D. On the use of two-dimensional-*J* NMR measurements for in vivo proton MRS: measurement of homonuclear decoupled spectra without the need for short echo times. Magn Reson Med 1995;34(3):331–7.

[4] von Kienlin M, et al. 2D-spatial/2D-spectral spectroscopic imaging of intracerebral gliomas in rat brain. Magn Reson Med 2000; 43(2):211–9.
[5] Mayer D, Dreher W, Leibfritz D. Fast U-FLARE-based correlation-peak imaging with complete effective homonuclear decoupling. Magn Reson Med 2003;49(5):810–6.
[6] Herigault G, et al. Multi-spin-echo *J*-resolved spectroscopic imaging without water suppression: application to a rat glioma at 7 T. Magma 2004;17(3–6):140–8.
[7] Jensen JE, et al. Two-dimensional, *J*-resolved spectroscopic imaging of GABA at 4 Tesla in the human brain. Magn Reson Med 2005;54(4):783–8.
[8] Mayer D, Dreher W, Leibfritz D. Fast echo planar based correlation-peak imaging: demonstration on the rat brain in vivo. Magn Reson Med 2000;44(1):23–8.
[9] Adalsteinsson E, Spielman DM. Spatially resolved two-dimensional spectroscopy. Magn Reson Med 1999;41(1):8–12.
[10] Hiba B, et al. 2D *J*-resolved spiral spectroscopic imaging at 7 T: application to mobile lipid mapping in a rat glioma. Magn Reson Med 2004;52(3):658–62.
[11] Kim DH, et al. In vivo prostate magnetic resonance spectroscopic imaging using two-dimensional *J*-resolved PRESS at 3 T. Magn Reson Med 2005;53(5):1177–82.
[12] Mayer D, et al. Fast CT-PRESS-based spiral chemical shift imaging at 3 Tesla. Magn Reson Med 2006;55(5):974–8.
[13] Srinivasan R, et al. TE-averaged two-dimensional proton spectroscopic imaging of glutamate at 3 T. Neuroimage 2006;30(4):1171–8.
[14] Dreher W, Leibfritz D. Improved proton spectroscopic U-FLARE imaging for the detection of coupled resonances in the rat brain in vivo. Magn Reson Imaging 1999;17(4):611–21.
[15] Glover GH. Simple analytic spiral *k*-space algorithm. Magn Reson Med 1999;42(2):412–5.
[16] Hurd R, et al. Measurement of brain glutamate using TE-averaged PRESS at 3T. Magn Reson Med 2004;51(3):435–40.
[17] Yue K, Chang L, Ernst T. Enhancing glutamine signals in TE-averaged PRESS spectra. ISMRM. Miami (FL): ISMRM; 2005. p. 2497.
[18] Kim DH, Spielman DM. Reducing gradient imperfections for spiral magnetic resonance spectroscopic imaging. Magn Reson Med 2006; 56:198–203.
[19] Kim D, Adalsteinsson E, Spielman D. Spiral-out spiral-in CSI. Toronto, Canada: ISMRM; 2003.
[20] Kim DH, et al. Regularized higher-order in vivo shimming. Magn Reson Med 2002;48(4):715–22.
[21] Dydak U, et al. Sensitivity-encoded spectroscopic imaging. Magn Reson Med 2001;46(4):713–22.
[22] Maudsley AA, et al. Reduced phase encoding in spectroscopic imaging. Magn Reson Med 1994;31(6):645–51.
[23] Gao Y, Reeves SJ. Optimal *k*-space sampling in MRSI for images with a limited region of support. IEEE Trans Med Imaging 2000;19(12): 1168–1178.
[24] Swanson MG, et al. Single-voxel oversampled *J*-resolved spectroscopy of in vivo human prostate tissue. Magn Reson Med 2001; 45(6):973–80.
[25] Ke Y, et al. Frontal lobe GABA levels in cocaine dependence: a two-dimensional, *J*-resolved magnetic resonance spectroscopy study. Psychiatry Res 2004;130(3):283–93.
[26] Cady EB, et al. Lactate, N-acetylaspartate, choline and creatine concentrations, and spin–spin relaxation in thalamic and occipito-parietal regions of developing human brain. Magn Reson Med 1996;36(6):878–86.
[27] Provencher SW. Automatic quantitation of localized in vivo 1H spectra with LCModel. NMR Biomed 2001;14(4):260–4.
[28] Govindaraju V, Young K, Maudsley AA. Proton NMR chemical shifts and coupling constants for brain metabolites. NMR Biomed 2000;13(3):129–53.
[29] Hurd RE, Gurr D, Sailasuta N. Proton spectroscopy without water suppression: the oversampled *J*-resolved experiment. Magn Reson Med 1998;40(3):343–7.
[30] Bolan PJ, et al. Eliminating spurious lipid sidebands in 1H MRS of breast lesions. Magn Reson Med 2002;48(2):215–22.
[31] Cunningham CH, et al. Design of flyback echo-planar readout gradients for magnetic resonance spectroscopic imaging. Magn Reson Med 2005;54(5):1286–9.
[32] Block KT, Frahm J. Spiral imaging: a critical appraisal. J Magn Reson Imaging 2005;21(6):657–68.
[33] Zierhut M, et al. Spectroscopic imaging of 1H of 3T: comparing SNR between traditional phase encoding and echo-planar techniques in the human brain. Seattle (WA): ISMRM; 2006.